Published in final edited form as:
Magn Reson Imaging. 2013 June ; 31(5): 669–675. doi:10.1016/j.mri.2012.10.017.

Conspicuity of Bone Metastases on Fast Dixon-Based Multisequence Whole Body MRI: Clinical Utility per Sequence

Colleen M. Costelloe, MD[1,*], **John E. Madewell, MD**[1], **Vikas Kundra, MD, PhD**[1], **Robyn K. Harrell, MS**[2], **Roland L. Bassett Jr., MS**[2], and **Jingfei Ma, PhD**[3]

[1]Department of Diagnostic Radiology, The University of Texas MD Anderson Cancer Center, Houston, Texas, USA

[2]Department of Biostatistics, The University of Texas MD Anderson Cancer Center, Houston, Texas, USA

[3]Department of Imaging Physics, The University of Texas MD Anderson Cancer Center, Houston, Texas, USA

Abstract

Purpose—To evaluate the conspicuity of bone metastases on each of the numerous sequences produced by fast Dixon-based multisequence whole-body (WB) MRI scanning in order to determine the most clinically useful sequences overall and per anatomic region.

Materials and Methods—Twenty-seven breast cancer patients with bone metastases were prospectively studied with fast Dixon-based WB MRI including head/neck, chest, abdominal, pelvic, thigh, calf/feet, and either cervical, thoracic and lumbar or cervical/thoracic and thoracic/lumbar regions. Sequences included coronal T2, axial T1 without and with intravenous gadolinium (+C), sagittal T1 spine +C, each associated fat only (FO) and fat saturated (FS) sequence, axial DWI and STIR. Blinded reviewers evaluated lesion conspicuity, a surrogate of clinical utility, on a 5 point scale per anatomic region. Sequences were compared using ANOVA, differences detected with Tukey's HSD, and the four sequences with highest mean conspicuity were compared to the remainder overall and per anatomic region.

[*]Please address reprint requests to Colleen M. Costelloe, MD.
Colleen M. Costelloe, MD, UT MD Anderson Cancer Center, 1515 Holcombe Blvd., Unit 1475, Houston, TX 77030, P: 713-563-1260, F: 713-563-6633, ccostelloe@mdanderson.org
John E. Madewell, MD, UT MD Anderson Cancer Center, 1515 Holcombe Blvd., Unit 1475, Houston, TX 77030, P: 713-792-4973, F: 713-563-6633, jmadewell@mdanderson.org
Vikas Kundra, MD, PhD, UT MD Anderson Cancer Center, 1515 Holcombe Blvd., Unit 1473, Houston, TX 77030, P: 713-745-2702, F: 713-794-4379, vkundra@mdanderson.org
Robyn K. Harrell, MS, McKesson Specialty Health, 10101 Woodloch Forest, The Woodlands, TX 77380, P: 281-863-6688, F: 832-348-5732, Robyn.Harrell@usoncology.com
Roland L. Bassett, Jr., MS, UT MD Anderson Cancer Center, 1515 Holcombe Blvd., Unit 1411, Houston, TX 77030, P: 713-563-4272, F: 713-563-4242, rlbassett@mdanderson.org
Jingfei Ma, PhD, UT MD Anderson Cancer Center, 1515 Holcombe Blvd., Unit 1472, Houston, TX 77030, P: 713-563-2713, F: 713-563-2720, jma@mdanderson.org

Conflict of interest
An author, Jingfei Ma, Ph.D., is the inventor of a United States of America patent on the fast Dixon sequences used in this study. No additional conflicts of interest of any kind exist regarding any other author.

Results—Overall, a significant lesion conspicuity difference was found (P<0.0001), and lesion conspicuity was significantly higher on FS T1 +C, FO T1 +C, T1 +C sagittal, FS T1 +C axial sequences (P<0.0001). Per region results were the same in head/neck. Other sequences overlapped with these and included: Chest/abdomen-FO T2, DWI; pelvis- DWI, FO T2; thigh-FS T2, FO T2, FO T1 +C; calf/feet-FS T2, DWI, FO T2, STIR.

Conclusion—Overall, bone lesions were most conspicuous on FS T1 +C sagittal, FO T1 +C sagittal, T1 +C sagittal and FS T1 +C axial fast Dixon WB MRI sequences.

Keywords

Whole Body MRI; Dixon; Breast Cancer; Bone; Metastases

1. Introduction

Whole-body (WB) MRI has been investigated for the detection of distant cancer metastases throughout the body on a single examination [1–3]. WB MRI has proven to be an effective method of evaluating the entire skeleton for bone metastases [4], which are common in patients with advanced breast cancer [5]. In comparison with other WB imaging modalities, MRI has the intrinsic advantage of providing excellent soft tissue contrast and high spatial resolution without the use of ionizing radiation. WB MRI is an evolving technique, and early studies included limited numbers of sequences [1, 2], thereby potentially compromising diagnostic accuracy.

More recently, investigators have successfully used two fast Dixon techniques, a fast spin echo triple echo Dixon (FTED) sequence [6] and a three-dimensional (3D) fast spoiled gradient echo dual echo Dixon (3D FSPGR-DE) sequence [7], to acquire coronal T2-weighted and axial T1-weighted images in a WB setting [8]. Breath-hold acquisitions can be performed with uniform water and fat separation despite the large-field inhomogeneity inherent to WB MRI. Large numbers of sequences can be performed in approximately 1 hour of total examination time [8]. For each individual fast Dixon T1- or T2-weighted acquisition, three types of images are generated [fat-only (FO), water-only, and in-phase (non-fat-suppressed (non-FS)] requiring no additional scan time and resulting in triple the number of sequences produced by using conventional MRI techniques. The greater variety of sequences can potentially increase the diagnostic efficacy of the scans [9]. For ease of discussion, the water-only sequences are interchangeably referred to as “FS T1” or “FS T2” and the in-phase sequences are interchangeably referred to as “T1” or “T2” in the remainder of the text.

WB MRI protocols commonly image the body by using 4–6 anatomic sections with multiple imaging planes per station. Each fast Dixon WB MRI study can therefore generate more than 50 sequences. Interpretation throughput is an important consideration regarding the cost-effectiveness of the scans [10], creating the need to find the sequences with the highest yield for detecting metastases. Identifying the sequences on which lesions were more conspicuous among the many sequences generated in a multisequence WB MRI study would allow radiologists to improve reading throughput. Therefore, we conducted the present study to determine the clinical utility of each sequence produced using the fast Dixon WB MRI technique and DWI for the detection of bone metastases in breast cancer patients using lesion conspicuity as an indicator of clinical utility. We expect the findings of this study to help in the selection of the highest-yield sequences for detection of bone metastases.

2. Materials and methods

2.1 Patients

This study was approved by the institutional review board, and all patients gave their written informed consent to participate. All patients had breast cancer and at least one bone metastasis on prior bone scan or biopsy, and no contraindications to MRI or intravenous gadolinium-based contrast agents. Subjects were identified by reviewing the Nuclear Medicine Department's patient schedule for follow-up bone scans. Twenty-seven female patients were prospectively accrued, and their ages ranged from 36 to 74 years (median 54 years). All patients were receiving therapy at the time of their scan.

2.2 Image acquisition

All WB MRI studies were performed using a commercially available 1.5 T whole-body scanner (Signa; GE Healthcare, Waukesha, WI) without any hardware modifications. The study protocol details were described previously [8] and scan parameters are listed in Table 1. Patients were imaged in a supine position using multiple table stations without repositioning. The scanner's radiofrequency body coil was used for all stations with the exception of T1- and T2-weighted imaging of the chest/abdomen and pelvis, for which an eight-element torso phased array coil was used to increase the signal-to-noise ratio. After scout images were obtained, axial DWI images were acquired using a short tau inversion recovery (STIR)-prepared DW sequence ($b = 500$ s/mm^2) [11]. The DW sequence also included an acquisition of $b = 0$ of each slice, which produced an equivalent STIR sequence. Coronal T2-weighted images with the FTED sequence [6] and precontrast axial T1-weighted images with the 3D FSPGR-DE sequence [7] were then obtained. Afterward, the patient table was moved to the abdomen station, where each patient received an injection of a single dose of gadolinium contrast (+ C). Postcontrast axial WB images and postcontrast sagittal spine images were acquired using the 3D FSPGR-DE sequence. For each acquisition, both FTED and 3D FSPGR-DE sequences were Dixon-based and produced a water-only, FO, and non-FS or combined water and fat image. The mean overall examination time was 68 minutes.

2.3 Image evaluation

The skeleton was segmented into the following anatomic regions based on the table stations: head/neck; chest/abdomen; pelvis; thigh; calf/feet; and either separate cervical, thoracic and lumbar spines or combined cervical/thoracic and thoracic/lumbar spines. A minimum of one bone lesion was required for evaluation of each anatomic region. When no lesions were identified in an anatomic region, the region was excluded from analysis. Each lesion was evaluated using a five-point visual scale for conspicuity (5 = extremely conspicuous, 4 = highly conspicuous, 3 = moderately conspicuous, 2 = not conspicuous, and 1 = not visible). A score of 5 was equated with the conspicuity of the urinary bladder on a T2-weighted, heavily fat saturated image (Fig. 1). When multiple bone lesions were present in a region, one conspicuous bone lesion was chosen randomly on sequences that were varied per anatomic region to avoid selection bias. The lesion was subsequently evaluated on each sequence obtained in the respective imaging plane of the anatomic region. Each anatomic region was evaluated independently.

WB MRI studies were evaluated by two musculoskeletal and one body radiologist. The reviewers were blinded to the results of all other imaging studies. Evaluations were performed in consensus, eliminating the possibility of discordant readings. The data for this study were obtained contemporaneously with a different investigation of the same images that evaluated the sensitivity and specificity of the WB MRI scans and bone scans as compared to reference imaging for the detection of bone metastasis. The separate evaluation

demonstrated 1 – > 72 bone metastases per patient and > 862 metastases overall [12]. While the reviewers were blinded to these results, they signify that a large number of bone metastases were present on the WB MRI scans. As per the expertise of the reviewers, lesions demonstrating signal intensity, morphology and location most consistent with metastases were evaluated.

2.4 Statistical analysis

2.4.1 Overall sequence analysis—The data from each anatomic region were combined so that the sequences could be assessed overall. Axial T1, axial FS T1, axial FO T1, axial T1 + C, axial FS T1 + C, axial FO T1 + C, coronal T2, coronal FS T2, coronal FO T2, axial DWI, and axial STIR sequences were included in the overall analysis. Sagittal spine sequences were also included and were acquired only after administration of the contrast agent using T1 + C, FS T1 + C, and FO T1 + C sequences. Additionally, some spines were scanned in two acquisitions (cervical/thoracic and thoracic/lumbar), whereas, others were scanned in three acquisitions (cervical, thoracic, and lumbar). Thus, the spine sequences were combined using the maximum conspicuity values of the two or three measurements, respectively. Therefore, the overall analysis included a total of 14 sequences (the 4 most conspicuous are included in Table 2). The conspicuity score (1–5) was analyzed as a continuous variable. For each sequence within a patient, the maximum conspicuity level across body segments was calculated, and these levels were compared among sequences by using analysis of variance (ANOVA). If a statistically significant difference among the sequences was found overall, Tukey's HSD test [13] was used to carry out all pairwise comparisons among sequences. As a result of the pairwise comparisons, an additional analysis was performed: the sequences with the four highest mean conspicuity values were compared with the remaining sequences using a linear contrast within ANOVA.

2.4.2 Anatomic region sequence analysis—The sequences were also analyzed according to anatomic region (head/neck, chest/abdomen, pelvis, thigh, calf/feet and sagittal spine). Due to anatomic overlap of the sagittal spines with other regions, some values were duplicated. When a patient's spine was scanned with two sagittal acquisitions, the thoracic/lumbar values were incorporated twice: first for the chest/abdomen region and also for the pelvis region. In these patients, the cervical/thoracic data was applied to the head/neck region. When a patient underwent three separate sagittal spine acquisitions (cervical and thoracic and lumbar), the first value was used for the head/neck region, the second value was used for the chest/abdomen region, and the third value was used for the pelvis. A total of 14 sequences were analyzed for the head/neck, chest/abdomen and pelvis regions. A total of 11 sequences were analyzed for the thigh and calf/feet stations because the sagittal C, T and L spine sequences were not applicable in those locations. The 4 most conspicuous sequences are included in Tables 3–7. The conspicuity score was also considered in this analysis as a continuous variable. For each region separately, as in the overall analysis, sequences were evaluated for overall differences in conspicuity score using ANOVA. If a statistically significant difference was observed, Tukey's HSD test was used to perform pairwise comparisons among the sequences to determine which sequences differed. Subsequently, the four sequences with the highest mean conspicuity values were compared with the remaining sequences using a linear contrast with ANOVA. The statistical significance level for all analyses was set at 0.05. With the exception of the Tukey HSD procedure that was used to adjust for multiplicity within each region, no additional adjustment was made for multiplicity between the regions. Computations were performed using the SAS software program (version 9; SAS Institute Inc., Cary, NC).

3. Results

3.1 Overall sequence analysis

We observed a statistically significant difference in lesion conspicuity among the sequences overall ($P < 0.0001$; ANOVA). Table 2 shows overall conspicuity by scan sequence. The top number in the cell refers to the count for that particular conspicuity score and the bottom number refers to the row percentage for that particular conspicuity score. Pairwise comparison demonstrated that the conspicuity values for the FS T1 + C sagittal (Fig. 2), FO T1 + C sagittal, T1 + C sagittal, and FS T1 + C axial sequences throughout the entire body were significantly higher than those for the other sequences ($P < 0.0001$; ANOVA).

3.2 Anatomic region sequence analysis

We found a significant difference in lesion conspicuity when they were analyzed only in the individual anatomic regions including the head/neck ($P < 0.0001$), chest/abdomen ($P = 0.0007$), pelvis ($P < 0.0001$), thighs ($P < 0.0001$) and calves/feet ($P = 0.0051$).

The four sequences with the highest lesion conspicuity in the following anatomic regions were significantly higher than the remainder of the sequences (Tables 3–7). An exception is that the sequences with the fourth and fifth highest conspicuity in the chest/abdomen region were equal. Head/neck, $P < 0.0001$, chest/abdomen $P < 0.0001$, pelvis $P < 0.0001$, thigh $P < 0.0001$, calves/feet $P < 0.0001$.

A large degree of overlap was found regarding the identity of the sequences with highest lesion conspicuity in the per-region and overall conspicuity analyses. The four sequences with the highest conspicuity in the head/neck region were the same as the overall (FS T1 + C sagittal, FO T1 + C sagittal, FS T1 + C axial and T1 + C sagittal, Table 3). The following regions contained one or more of the sequences that were identified in the overall analysis plus those that are listed: Chest/abdomen-FO T2 coronal, DWI axial, Table 4; pelvis- DWI axial, FO T2 coronal, Table 5; thigh-FS T2 coronal, FO T2 coronal, FO T1 +C axial, Table 6. The sequences with highest conspicuity in the calf/feet section were FS T2 coronal, DWI axial, FO T2 coronal and STIR axial, Table 7.

In summary, Table 8 lists the sequences with the most conspicuous lesions overall and in the per-region analysis.

4. Discussion

Use of the fast Dixon-based techniques for whole-body scanning is increasing in popularity and has been investigated for indications such as the detection of bone metastases in breast cancer patients [8, 12], scanning obese patients in whom fat suppression is otherwise difficult [14], and variations of the Dixon technique have been used for rapid whole body scanning of pediatric patients [15]. T1-weighted sequences following the administration of intravenous gadolinium-based contrast have been incorporated into numerous other WB MRI protocols [16–19] and its usage is validated in the current study. We found that the fast Dixon-based WB MRI technique used in our study permitted this and many other sequences to be applied in the sagittal, coronal and axial plane in approximately 1 hour of total scan time. Additionally, among the contrast-enhanced sequences, we observed significantly high conspicuity more often with than without fat saturation.

The availability of a combination of sequences can increase diagnostic confidence for the identification of bone metastases (Fig. 3). However, our study showed that the sequences did not all provide the same level of lesion conspicuity and that the sequences with greatest conspicuity differed according to anatomic region. In the majority of anatomic regions

containing the spine (head/neck, chest/abdomen, pelvis), sagittal sequences often had the greatest lesion conspicuity. This likely resulted from the anatomic configuration of the spine, and is of particular importance because the spine is the site of the greatest number of bone metastases [20]. These results support the inclusion of sagittal spine sequences in WB MRI scans used for the detection of bone metastases.

DW images are sensitive to Brownian motion of water molecules and provide image contrast that is different from those of the traditional T1 and T2-weighted sequences. For WB MRI, DW images have been shown to be useful in detecting cancer metastases, such as to bone and lymph nodes. However, DW images generally have low spatial resolution, and echo planar imaging pulse sequences (on which our DWI sequence was based) are very susceptible to image artifacts (e.g., magnetic field inhomogeneity, motion). This could explain why the DW sequence in our study provided high conspicuity only in the pelvis.

Limitations of our study included a relatively small number of patients and evaluation of one lesion per sequence in each anatomic region. Nevertheless, we evaluated a large number of sequences per region (1228 sequences)). The optimal method of evaluation would have been to analyze each lesion independently. However, such an analysis would have been prohibitively lengthy because of large numbers of lesions in most patients and the large number of sequences acquired. All patients were receiving therapy at the time of their scan. Variation in the effectiveness of therapy is expected. Treated metastases likely have lower water content and may be more conspicuous on FO images. Metastases that did not respond or had not yet responded are likely to have better vascular perfusion and are more likely to enhance or be higher in T2 signal than metastases that are effectively treated. This may help to explain the differing sequences upon which we found lesions to be most conspicuous. Our results are expected to be helpful in patients with treated and untreated bone metastases and can be further evaluated with future research.

5. Conclusion

In conclusion, FS T1 + C sagittal, FO T1 + C sagittal, T1 + C sagittal, and FS T1 + C axial sequences had significantly higher conspicuity values for bone metastases than did the other sequences overall, and were often also found to provide high lesion conspicuity when anatomic regions were evaluated individually. The results of this study suggest that these four sequences should be given priority in interpretation of fast Dixon-based WB MRI studies performed for the detection of bone metastases.

Acknowledgments

The authors thank Donald Norwood, Scientific Editor, Department of Scientific Publications.

Grant support

Susan G. Komen for the Cure Research Foundation; this research was also supported in part by the National Institutes of Health through the University of Texas MD Anderson Cancer Center Support Grant CA016672.

Role of the funding source

Neither the Komen Foundation nor the National Institutes of Health influenced the research.

References

1. Eustace S, Tello R, DeCarvalho V, Carey J, Wroblicka JT, Melhem ER, et al. A comparison of whole-body turboSTIR MR imaging and planar 99mTc-methylene diphosphonate scintigraphy in the examination of patients with suspected skeletal metastases. AJR Am J Roentgenol. 1997; 169(6):1655–1661. [PubMed: 9393186]

2. Walker R, Kessar P, Blanchard R, Dimasi M, Harper K, DeCarvalho V, et al. Turbo STIR magnetic resonance imaging as a whole-body screening tool for metastases in patients with breast carcinoma: preliminary clinical experience. J Magn Reson Imaging. 2000; 11(4):343–350. [PubMed: 10767062]
3. Heusner T, Golitz P, Hamami M, Eberhardt W, Esser S, Forsting M, et al. “One-stop-shop” staging: should we prefer FDG-PET/CT or MRI for the detection of bone metastases? Eur J Radiol. 2011; 78(3):430–435. [PubMed: 19945240]
4. Lauenstein TC, Freudenberg LS, Goehde SC, Ruehm SG, Goyen M, Bosk S, et al. Whole-body MRI using a rolling table platform for the detection of bone metastases. Eur Radiol. 2002; 12(8): 2091–2099. [PubMed: 12136329]
5. Abrams HL, Spiro R, Goldstein N. Metastases in carcinoma; analysis of 1000 autopsied cases. Cancer. 1950; 3(1):74–85. [PubMed: 15405683]
6. Ma J, Son JB, Zhou Y, Le-Petross H, Choi H. Fast spin-echo triple-echo dixon (fTED) technique for efficient T2-weighted water and fat imaging. Magn Reson Med. 2007; 58(1):103–109. [PubMed: 17659631]
7. Ma J, Vu AT, Son JB, Choi H, Hazle JD. Fat-suppressed three-dimensional dual echo Dixon technique for contrast agent enhanced MRI. J Magn Reson Imaging. 2006; 23(1):36–41. [PubMed: 16315212]
8. Ma J, Costelloe CM, Madewell JE, Hortobagyi GN, Green MC, Cao G, et al. Fast dixon-based multisequence and multiplanar MRI for whole-body detection of cancer metastases. J Magn Reson Imaging. 2009; 29(5):1154–1162. [PubMed: 19388121]
9. Nakanishi K, Kobayashi M, Nakaguchi K, Kyakuno M, Hashimoto N, Onishi H, et al. Whole-body MRI for detecting metastatic bone tumor: diagnostic value of diffusion-weighted images. Magn Reson Med Sci. 2007; 6(3):147–155. [PubMed: 18037795]
10. van den Biggelaar FJ, Kessels AG, van Engelshoven JM, Flobbe K. Costs and effects of using specialized breast technologists in prereading mammograms in a clinical patient population. Int J Technol Assess Health Care. 2009; 25(4):505–513. [PubMed: 19845980]
11. Takahara T, Imai Y, Yamashita T, Yasuda S, Nasu S, Van Cauteren M. Diffusion weighted whole body imaging with background body signal suppression (DWIBS): technical improvement using free breathing, STIR and high resolution 3D display. Radiat Med. 2004; 22(4):275–282. [PubMed: 15468951]
12. Costelloe CM, Kundra V, Ma J, Chasen BA, Rohren EM, Bassett RL Jr, et al. Fast dixon whole-body MRI for detecting distant cancer metastasis: A preliminary clinical study. J Magn Reson Imaging. 2012; 35:399–408. [PubMed: 21990095]
13. Tukey, JW. The Collected Works of John W. Tukey VIII. Multiple Comparisons: 1948–1983. Chapman and Hall; New York: 1951. Reminder sheets for “Discussion of paper on multiple comparisons by Henry Scheffé”.
14. Berglund J, Johansson L, Ahlstrom H, Kullberg J. Three-point Dixon method enables whole-body water and fat imaging of obese subjects. Magn Reson Med. 2010; 63(6):1659–1668. [PubMed: 20512869]
15. Vasanawala SS, Madhuranthakam AJ, Venkatesan R, Sonik A, Lai P, Brau AC. Volumetric fat-water separated T2-weighted MRI. Pediatr Radiol. 2011; 41(7):875–883. [PubMed: 21243349]
16. Ohno Y, Koyama H, Onishi Y, Takenaka D, Nogami M, Yoshikawa T, et al. Non-small cell lung cancer: whole-body MR examination for M-stage assessment--utility for whole-body diffusion-weighted imaging compared with integrated FDG PET/CT. Radiology. 2008; 248(2):643–654. [PubMed: 18539889]
17. Thomson V, Pialat JB, Gay F, Coulon A, Voloch A, Granier A, et al. Whole-body MRI for metastases screening: a preliminary study using 3D VIBE sequences with automatic subtraction between noncontrast and contrast enhanced images. Am J Clin Oncol. 2008; 31(3):285–292. [PubMed: 18525309]
18. Takenaka D, Ohno Y, Matsumoto K, Aoyama N, Onishi Y, Koyama H, et al. Detection of bone metastases in non-small cell lung cancer patients: comparison of whole-body diffusion-weighted imaging (DWI), whole-body MR imaging without and with DWI, whole-body FDG-PET/CT, and bone scintigraphy. J Magn Reson Imaging. 2009; 30(2):298–308. [PubMed: 19629984]

19. Heusner TA, Kuemmel S, Koeninger A, Hamami ME, Hahn S, Quinsten A, et al. Diagnostic value of diffusion-weighted magnetic resonance imaging (DWI) compared to FDG PET/CT for whole-body breast cancer staging. Eur J Nucl Med Mol Imaging. 2010; 37(6):1077–1086. [PubMed: 20204355]

20. Clain A. Secondary Malignant Disease of Bone. Br J Cancer. 1965; 19:15–29. [PubMed: 14284378]

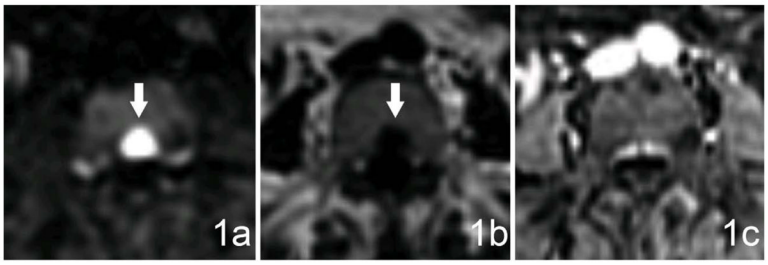

Figure 1.

Examples of the conspicuity scale in a 53 year old woman with breast cancer. (a) A bone lesion in the posterior aspect of the L4 vertebral body demonstrates restricted diffusion, is highly conspicuous (arrows), and has a score of 5 on the five-point conspicuity scale. (b) The same lesion is slightly less conspicuous on the FO image generated during the same T1-weighted fast Dixon-based acquisition and has a score of 3 on the conspicuity scale. (c) The lesion is not visible on the FS T1-weighted + C image and thus has a score of 1 on the conspicuity scale. The bone lesions in our study exhibited variable conspicuity on different sequences, and the same patient often had multiple lesions with widely varying conspicuity patterns. The differing lesion conspicuity on the various sequences exemplified the need for obtaining multiple sequences in order to increase the likelihood of effectively detecting bone metastases.

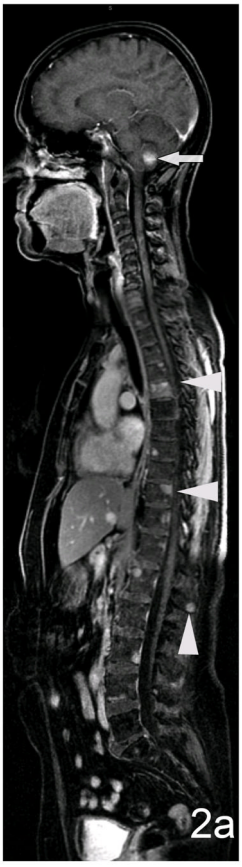

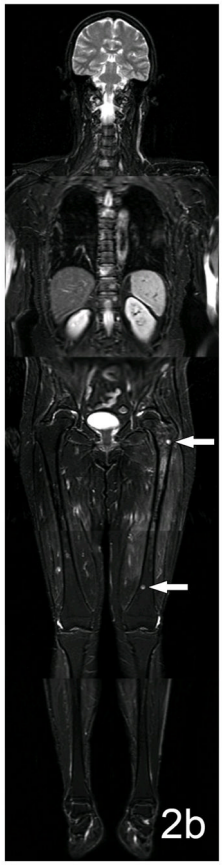

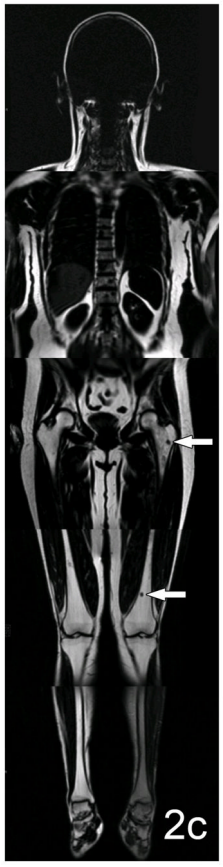

Figure 2.

Sagittal and coronal composite images demonstrating whole-body lesion conspicuity. Figure (a), is a sagittal composite of FS T1 + C images in this 55 year old woman with breast cancer and is the sequence upon which bone metastases were most conspicuous in the study. Enhancing metastases in numerous vertebral bodies are readily apparent on a background of darkly saturated fat. Three of the most conspicuous bone metastases are indicated (arrowheads) and rank 4–5 on the conspicuity scale. An enhancing brain metastasis is incidentally detected (arrow). On the coronal composite images (b, c) focal metastases in the spine and proximal and distal left femur are shown (arrows). The lesions on the coronal FS T2-weighted image (b) are bright on a background of saturated fat. The lesion in the proximal left femur (upper arrow) enhances well, is highly conspicuous and ranked a score of 5 on the conspicuity scale. The lesion in the distal femur (lower arrow) is less conspicuous and ranks a 4. The lesions on the coronal FO sequences generated during the same acquisition (c) are dark on a background of bright fat. The lesion in the proximal femur is now ranked a 4 on the conspicuity scale because adjacent red marrow is also dark on FO images and the overall effect is to decrease the conspicuity of the lesion. Nevertheless, the lesion in the distal femur is surrounded by fatty yellow marrow and now is ranked 5 because of the high conspicuity produced between the dark lesion and the bright yellow marrow.

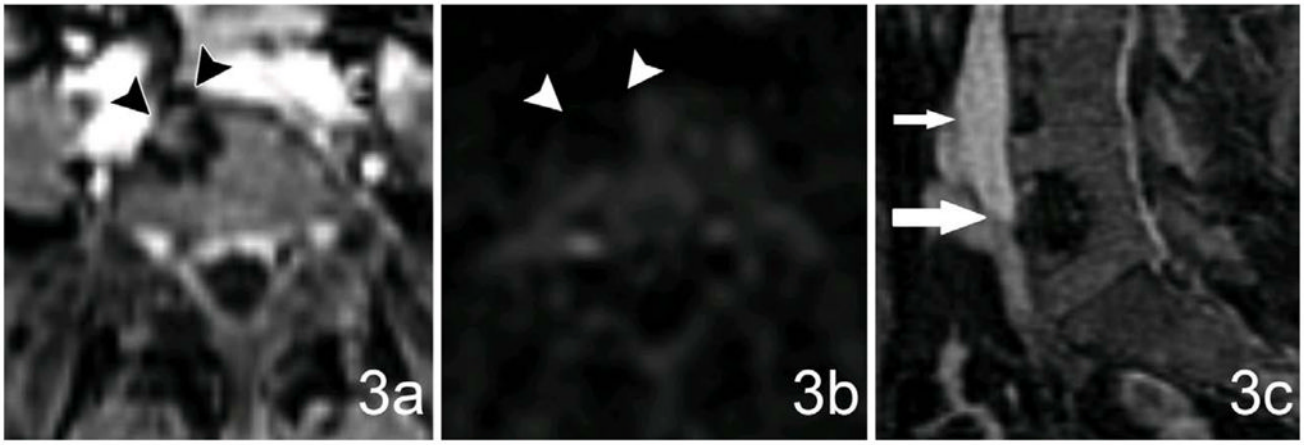

Figure 3.

The advantage of multisequence and multiplanar imaging in the same patient shown in Fig. 1. (a) A heterogeneously enhancing lesion is seen in the anterior aspect of the L5 vertebral body on the axial FS T1 + C sequence (conspicuity score of 4 on the five-point scale, arrowheads), (b) is dark and difficult to discern on the axial DWI sequence (conspicuity score of 2, arrowheads). This is the opposite of the lesion's conspicuity pattern in the L4 vertebral body in Fig. 1, exemplifying the utility of multiple sequences for lesion detection. The dark periphery of the lesion on the axial FS T1 + C sequence raises the possibility of a degenerative Schmorl node (disc herniation into a vertebral body) with a rim of sclerosis. (c) On the sagittal FS T1 + C sequence, the epicenter of the lesion is in the center of the vertebral body (large arrow), not at the end plate. Therefore, multiplanar imaging aids in the diagnosis of a bone metastasis rather than degenerative change. The multiplicity of lesions also aids in the diagnosis of bone metastases (arrow). As expected, the lesion in the posterior aspect of the L4 body (Fig. 1) is not visible on the sagittal FS T1 + C sequence.

Table 1

Fast Dixon-based WB MRI Protocol Specifics

Sequence	Anatomic Segment		Parameter								
			Scan plane	TR (ms)	TE (ms)	Matrix	Slice/Gap (mm)	# of slices per acquisition	FOV (cmxcm)	NEX	Scan time (minute)
Localizer	4 segments		Axial								0:52
DWI and STIR	6 segments		Axial	4500	57	128×128	8/−1	39	48×48	4	3:43×6=22:18
FTED T2W	Head/shoulder		Coronal	6500	80	256×192	6/1	16	34×34	1	1:25
	Chest/abdomen		Coronal	2500	80	256×160	7/1	12×2	48×48	1	0:24×2 = 0:48
	Pelvis		Coronal	6000	80	256×192	6/1	28	48×48	2	2:30
	Thigh		Coronal	5400	80	256×192	6/1	26	48×48	2	2:15
	Calf		Coronal	7650	80	256×192	5/1	26	46×46	2	3:11
FSPGR-DE T1W	Head/shoulder	Pre and post contrast injection	Axial	6.7	2.2/4.6	256×192	5/0	28	34×26	0.78	0:44×2 =1:28
	Chest		Axial	6.7	2.2/4.6	256×160	5/0	28	48×29	0.78	0:24×2 = 0:48
	Pelvis		Axial	6.7	2.2/4.6	256×160	5/0	34	48×33	0.78	0:37×2 = 1:14
	Thigh		Axial	6.7	2.2/4.6	256×192	5/0	34	48×33	0.78	1:05×2 = 2:10
	Calf		axial	6.7	2.2/4.6	256×192	5/0	52	42×29	0.78	1:11×2 = 2:22
	Head/C-spine		Sagittal	6.7	2.2/4.6	256×192	4/0	22	30×30	1.58	1:44
	CT-spine		Sagittal	6.7	2.2/4.6	256×192	4/0	16	36×28	0.8	0:25
	TL-spine		Sagittal	6.7	2.2/4.6	256×192	4/0	16	34×30	1.6	0:53
									Total scan time		45:20

DWI = diffusion weighted imaging, FTED= fast spin echo triple echo Dixon, FSPGR-DE = fast spoiled gradient echo dual echo Dixon, C = cervical, CT = cervical and thoracic, TL = thoracic and lumbar Q9

Table 2

Overall Sequence Conspicuity

Sequence*	Conspicuity Ranking Scale (number of segments, percent)					Total	Mean
	1	2	3	4	5		
FS T1 +C sagittal	1 (4.00%)	2 (8.00%)	2 (8.00%)	6 (24.00%)	14 (56.00%)	25	4.20
FO T1 + C sagittal	0 (0.00%)	1 (4.00%)	7 (28.00%)	12 (48.00%)	5 (20.00%)	25	3.84
T1 + C sagittal	1 (4.00%)	0 (0.00%)	10 (40.00%)	12 (48.00%)	2 (8.00%)	25	3.56
FS T1 + C axial	6 (6.45%)	7 (7.53%)	26 (27.96%)	38 (40.86%)	16 (17.20%)	93	3.55

FO = fat only, FS = fat saturated, + C = intravenous gadolinium contrast administration

*The sequences shown were significantly different from the remainder (not shown)

Table 3

Head/Neck Sequence Conspicuity

Sequence*	Conspicuity Ranking Scale (number of segments, percent)					Total	Mean
	1	2	3	4	5		
FS T1 +C sagittal	2 (9.52%)	2 (9.52%)	7 (33.33%)	3 (14.29%)	7 (33.33%)	21	3.52
FO T1 +C sagittal	1 (4.76%)	2 (9.52%)	7 (33.33%)	7 (33.33%)	4 (19.05%)	21	3.52
FS T1 +C axial	1 (6.25%)	1 (6.25%)	5 (31.25%)	8 (50.00%)	1 (6.25%)	16	3.44
T1 + C sagittal	2 (9.52%)	4 (19.05%)	6 (28.57%)	8 (38.10%)	1 (4.76%)	21	3.10

FO = fat only, FS = fat saturated, + C = intravenous gadolinium contrast administration

*The sequences shown were significantly different from the remainder (not shown)

Table 4

Chest/Abdomen Sequence Conspicuity

Sequence*	Conspicuity Ranking Scale (number of segments, percent)					Total	Mean
	1	2	3	4	5		
FS T1 + C sagittal	1 (4.35%)	2 (8.70%)	4 (17.39%)	10 (43.48%)	6 (26.09%)	23	3.78
FO T2 coronal	3 (11.54%)	3 (11.54%)	4 (15.38%)	11 (42.31%)	5 (19.23%)	26	3.46
FS T1 + C axial	1 (4.00%)	3 (12.00%)	7 (28.00%)	12 (48.00%)	2 (8.00%)	25	3.44
DWI axial	4 (17.39%)	2 (8.70%)	4 (17.39%)	6 (26.09%)	7 (30.43%)	23	3.43
FO T1 + C sagittal	1 (4.35%)	4 (17.39%)	3 (13.04%)	14 (60.87%)	1 (4.35%)	23	3.43

DWI = diffusion-weighted imaging, FO = fat only, FS = fat saturated, + C = intravenous gadolinium contrast administration

*The sequences shown were significantly different from the remainder (not shown)

Table 5

Pelvis Sequence Conspicuity

Sequence*	Conspicuity Ranking Scale (number of segments, percent)					Total	Mean
	1	2	3	4	5		
DWI axial	1 (4.35%)	0 (0.00%)	3 (13.04%)	10 (43.48%)	9 (39.13%)	23	4.13
FS T1 + C axial	1 (4.17%)	1 (4.17%)	6 (25.00%)	9 (37.50%)	7 (29.17%)	24	3.83
FS T1 + C sagittal	1 (4.17%)	2 (8.33%)	4 (16.67%)	12 (50.00%)	5 (20.83%)	24	3.75
FO T2 coronal	0 (0.00%)	5 (21.74%)	4 (17.39%)	6 (26.09%)	8 (34.78%)	23	3.74

DWI = diffusion-weighted imaging, FO = fat only, FS = fat saturated, + C = intravenous gadolinium contrast administration

*The sequences shown were significantly different from the remainder (not shown)

Table 6

Thigh Sequence Conspicuity

Sequence*	Conspicuity Ranking Scale (number of segments, percent)					Total	Mean
	1	2	3	4	5		
FS T1 + C axial	0 (0.00%)	1 (5.56%)	5 (27.78%)	7 (38.89%)	5 (27.78%)	18	3.89
FS T2 coronal	1 (5.88%)	1 (5.88%)	3 (17.65%)	9 (52.94%)	3 (17.65%)	17	3.71
FO T2 coronal	0 (0.00%)	2 (12.50%)	5 (31.25%)	6 (37.50%)	3 (18.75%)	16	3.63
FO T1 + C axial	1 (5.56%)	3 (16.67%)	2 (11.11%)	9 (50.00%)	3 (16.67%)	18	3.56

FO = fat only, FS = fat saturated, + C = intravenous gadolinium contrast administration

*The sequences shown were significantly different from the remainder (not shown)

Table 7

Calf/Feet Sequence Conspicuity

Sequence*	Conspicuity Ranking Scale (number of segments, percent)					Total	Mean
	1	2	3	4	5		
FS T2 coronal	0 (0.00%)	2 (20.00%)	1 (10.00%)	5 (50.00%)	2 (20.00%)	10	3.70
DWI axial	2 (20.00%)	2 (20.00%)	1 (10.00%)	1 (10.00%)	4 (40.00%)	10	3.30
FO T2 coronal	0 (0.00%)	4 (40.00%)	2 (20.00%)	3 (30.00%)	1 (10.00%)	10	3.10
STIR axial	3 (30.00%)	1 (10.00%)	1 (10.00%)	3 (30.00%)	2 (20.00%)	10	3.00

DWI = diffusion-weighted imaging, FO = fat only, FS = fat saturated, STIR = short tau inversion recovery, + C = intravenous gadolinium contrast administration

*The sequences shown were significantly different from the remainder (not shown)

Table 8

Summary of Sequence Conspicuity

Region	Most conspicuous	Second highest conspicuity	Third highest conspicuity	Fourth highest conspicuity
Overall	FS T1 +C sagittal	FO T1 + C sagittal	T1 + C sagittal	FS T1 + C axial
Head/Neck	FS T1 + C sagittal	FO T1 + C sagittal	FS T1 + C axial	T1 + C sagittal
Chest/Abdomen	FS T1 + C sagittal	FO T2 coronal	FS T1 + C axial	DWI axial * FO T1 + C sagittal *
Pelvis	DWI axial	FS T1 + C axial	FS T1 + C sagittal	FO T2 coronal
Thigh	FS T1 + C axial	FS T2 coronal	FO T2 coronal	FO T1 + C axial
Calf/Feet	FS T2 coronal	DWI axial	FO T2 coronal	STIR axial

DWI = diffusion-weighted imaging, FO = fat only, FS = fat saturated, STIR = short tau inversion recovery, + C = intravenous gadolinium contrast administration,

* tie